Jurnal Kejuruteraan 36(5) 2024: 2063–2074
https://doi.org/10.17576/jkukm-2024-36(5)-24

Dynamic Modelling and Validation of Tracked Vehicle with In-Track Motor

Noor Amira Ilyanie Ruslan[b] , Noor Hafizah Amer[a,b*] , Nurulhani Adlina Madzan[c] , Khisbullah Hudha[b], Zulkiffli Abd. Kadir[b] , Syed Mohd Fairuz Syed Mohd Dardin[c] & Saiddi Ali Firdaus Mohamed Ishak[b]

[a]*Centre of Defense Research and Technology,*
National Defence University of Malaysia,
Kem Sungai Besi, 57000 Kuala Lumpur, Malaysia,

[b]*Department of Mechanical Engineering, Faculty of Engineering,*
National Defence University of Malaysia,
Kem Sungai Besi, 57000 Kuala Lumpur, Malaysia

[c]*Department of Electrical and Electronic Engineering, Faculty of Engineering,*
National Defence University of Malaysia,
Kem Sungai Besi, 57000 Kuala Lumpur, Malaysia,

**Corresponding author: noorhafizah@upnm.edu.my*

Received 28 February 2024, Received in revised form 9 June 2024
Accepted 10 July 2024, Available online 30 September 2024

ABSTRACT

This paper addresses dynamic modelling and validation of a tracked vehicle, as well as provides an in-depth examination of an in-track DC motor system. The characteristics of the DC motor will be rigorously assessed, providing a foundational understanding to enhance vehicle control and mobility. Furthermore, an independent DC motor controller will be developed through an inverse model database of its characteristics. The model validation process will involve various trajectory types, including right and left turns. The real vehicle was equipped with an Arduino Mega and MPU6050 accelerometer sensor, along with the DC motor controller unit. Data acquisition was developed by integrating Arduino and the MATLAB/Simulink simulation environment. The proposed model was validated by evaluating the Root Mean Square (RMS) of the percentage error between the values of the experiment and the model prediction. It was found that, for right and left turns of the vehicle, the percentage error produced is below 12.7% which shows the model is able to follow the path in real conditions, providing a foundation for future advancements in transportation and autonomous technology.

Keywords: Tracked vehicle; dynamic modelling; independent DC motor controller; vehicle model validation

INTRODUCTION

Tracked vehicles have been developed to enhance mobility across a variety of challenging terrains, such as snow, loose sand, mud, and steep slopes combinations. Traditional wheeled vehicles would struggle to navigate through such environments (Sebastian & Ben-Tzvi 2019). Vehicles equipped with tracks are the preferred choice for these conditions due to their ability to operate effectively in hazardous terrains. They offer numerous advantages, including exceptional traction, even on slippery surfaces, robust load-bearing capabilities, and efficient power delivery. This type of design is more robust than the wheeled vehicles and it can easily perform sharp turns at a tight radius regardless of the smoothness of the surface and the type of the terrain. Given their superior traction in comparison to wheeled vehicles, tracked vehicles are the optimal choice for tasks that require substantial grip (Ugenti et al. 2023)-(Salah & Al-Jarrah 2019). Consequently, tracked vehicles have been developed to address various needs in civilian and also military sectors.

Furthermore, tracked vehicles have found extensive usage in a variety of agricultural activities, such as planting, harvesting, and transporting crops (Saito et al. 2013; Wenju

et al. 2022; Y. Yang et al. 2023). The significant benefit in this area is ability of tracked vehicles to relieve soil compaction, because the vehicle spread its weight in a more even manner, eliminating soil compaction and harm to both crops and soil structure. Additionally, tracked vehicles hold a crucial position within military sectors due to their exceptional off-road mobility and superior all-terrain capabilities. This allows them to navigate terrains that would be insurmountable for wheeled vehicles, and their capacity to transport heavy loads, deploy weaponry, and sustain operational readiness across varied environments solidifies their pivotal role in military logistics and combat operations (Yang et al. 2023).

Developing a vehicle model is a crucial step in simulating vehicle behaviours and formulating a control strategy. Usually, both dynamic and kinematic vehicle models are used. The dynamic model considers internal forces, inertia, and energy components for motion analysis, while the kinematic model concentrates on a vehicle's motion characteristics in relation to its geometric properties (Ruslan et al. 2023). Depending on the intended application and desirable characteristics for analysis, each model setup has its own benefits and functions. In this study, the dynamic type of tracked vehicle model is developed referring to previous researchers (Le et al. 2006; Zou et al. 2018) which considers tractive and resistance forces acting on the vehicle's track.

In addition, many kinds of tracked vehicles have evolved over time, as a result of technological advancements, developing increasingly complex and advanced vehicles. In any case, the rotational power from the main powertrain of the vehicle is supplied to both the left and right tracks, which are the primary sources of traction. Meanwhile, conventional tracked vehicles predominantly rely on internal combustion engines (ICE) that generate power through fuel combustion, recent technological progress had increased the interest towards electric-powered tracked vehicles, employing two DC motors on each track to convert electrical energy into mechanical energy for track propulsion (Al-Jarrah 2019; Sivakumar et al. 2017). DC motors provide benefits like improved effectiveness, precise control, and lower emissions, serving as a viable option compared to conventional ICE-powered tracked vehicles. When formulating control strategies for DC motors, there are commonly utilised methods, typically classified as open-loop or closed-loop controllers, with most DC motor controllers falling into the closed-loop category (Adli et al. 2018; Auliansyah et al. 2020; Ma'Arif et al. 2020; Naik et al. 2021; Sultan et al. 2019; Vikhe et al. 2019).

Previously in several research, validation process was carried out by comparing the reference and the actual trajectory of the tracked vehicle in X-Y coordinates. Jiao et al. (2018) had validated the proposed controller for trajectory tracking of DC motor on an agricultural tracked robots in X-Y global coordinates by varying the angular velocities for left and right tracks driving motors to control the movement of the tracked robot. On top of that, using the same methods of validation, the dynamic model of unmanned tracked vehicles was validated (Zou et al. 2018). The X-Y coordinate method in validating the proposed controller of the tracked vehicles is also used by these researchers in their studies (Hu & Cheng, 2023; Sabiha et al. 2022; Wang et al. 2022). Therefore, in this study, the validations on trajectory of the dynamic tracked vehicle in global X-Y coordinates for two types of paths which are turning to right, and left is measured.

Based on the reviewed studies, it can be seen that numerous studies have been performed on tracked vehicle autonomous control, especially on vehicle modelling, electric powertrain, and its subsequent control strategies for DC motor. In the vehicle control studies, most of vehicle modelling techniques were employing kinematic approach which pose challenges in studies involving kinetic parameter studies. Those studies that did employ dynamic model was focusing on ICE-powered tracked vehicle. For vehicles with electrical powertrain, this model will need to be enhanced with a DC motor integration. To do this, a good DC motor control strategies should be developed. Most of the studies were employing a closed-loop control strategy instead of open-loop. Even though closed-loop controllers offer more stable and accurate control system, the open-loop controller itself is important in the basic for developing the control system. Therefore, the independent DC motor controller is developed in this study.

The contribution of this study lies on the aspects of the controller: i) DC motor used on the tracked vehicle powertrain has been characterised using a new approach that involves the development of channel mapping and inverse database; ii) dynamic vehicle model for tracked vehicle has been developed and validated against a tracked vehicle that incorporates in-track DC motor instead of previous kinematic models and models for vehicles with ICEs. The main aim of this study is to develop and validate a dynamic tracked vehicle model. First, the development of the tracked vehicle model from previous researchers is developed in MATLAB-Simulink. After that, the developed independent DC motor controller is then validated by obtaining the response on predicted and actual angular speed of both tracks. The proposed independent motor controller is an open-loop type controller. However, the accuracy and stability of the open-loop type controller can be improved by modelling an accurate system to reduce the prediction error of the controller. Moreover, the independent DC motor controller is beneficial since it is easy, simple and generally stable. Next, the vehicle model

is then validated by observing the response of the tracked vehicle in global X-Y coordinates which this method is mostly used by other researchers and also gives the real behaviour of the tracked vehicle manoeuvrings.

The paper is structured as follows: In the first section, an overview of prior vehicle modelling and the validation process for tracked vehicles is discussed. The second section elaborates on the development of the DC motor model and validates its characteristics. Moving on, the third section details the proposed DC motor controller, with an assessment of its performance used to determine the input parameters for the model by comparing RMS of the percentage errors. In the fourth section, the validation of the developed vehicle model is discussed, specifically in terms of its trajectory. Finally, the fifth section presents the overall conclusions of this study.

DEVELOPMENT OF DYNAMIC TRACKED VEHICLE MATHEMATICAL MODEL

A dynamic vehicle model encompasses internal forces, energy, or momentum within its framework, allowing for the representation of the vehicle's movement in terms of position, velocity, and acceleration. Furthermore, this model considers the interaction of forces between the vehicle's tracks and the ground, thereby accounting for the resultant forces generated. Additionally, the frequently used method to derive the mathematical model of tracked vehicle dynamics is the Newtonian equation of motions. This vehicle model is developed with 3 degrees of freedom that considers the yaw rate, longitudinal and lateral motions of the tracked vehicle. Figure 1 shows the tracked vehicle model which illustrates all the forces present in a tracked vehicle.

The dynamic model for tracked vehicles involves a set of equations, as depicted in (1)-(3) (Le et al. 2006; Sabiha et al. 2022; Zou et al. 2018). These equations encompass various parameters such as the vehicle's mass, its moment of inertia about the z-axis, I the longitudinal acceleration in the x-direction, $\ddot{x}$ and the lateral acceleration in the y-direction, $\ddot{y}$ and the yaw acceleration about z-axis, $\ddot{\psi}$. These equations account for multiple forces, including the tractive forces acting on the left and right tracks of the tracked vehicle, F_L and F_R, which are influenced by the interaction between the track and soil resulting from the soil's shear stress. Additionally, the equations consider the resistance forces, R_L and R_R experienced by the left and right tracks, respectively. In lateral direction, the model considers a uniformly distributed lateral force per unit length, f_y, distance between the instantaneous center of rotation and the center of gravity, d_s, and b and l are the half width and half length of the vehicle as shown in Figure 1.

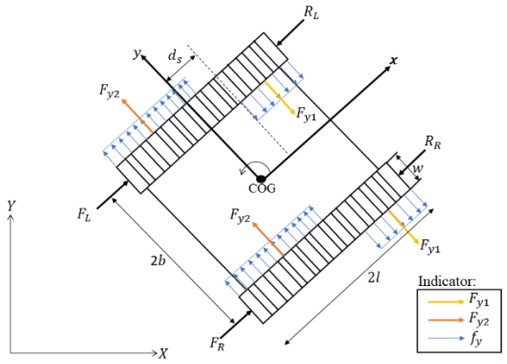

FIGURE 1. Force model of a tracked vehicle

$$\ddot{x} = \frac{1}{m}(F_R + F_L - R_L - R_R) \tag{1}$$

$$\ddot{y} = \frac{1}{m}(4 f_y d_s) \tag{2}$$

$$\ddot{\psi} = \left[(F_R - R_R)b - (F_L - R_L)b - 2f_y(l^2 - d_s^2)\right]\frac{1}{I} \tag{3}$$

Next, tractive force is the traction on the tracks applied to the ground which moves parallel to its direction of motion (Ahmadi et al. 2000). The equations used to determine the tractive force of the left and right tracks of the vehicle is shown in (4). Moreover, the maximum tractive effort, F_{max} is determined by the contact area, A and the shear strength of the terrain, τ_{max} as derived in equation (5), where C represent the apparent cohesion, ψ stands for the angle of internal friction of the soil, and P signifies the normal pressure beneath the track. Meanwhile, the slips of the vehicle occurring on the left and rights tracks are calculated using equations (6)-(8). Here, $V_{jL/R}$ represents the slip velocity of both left and right tracks, r denotes as sprocket radius, ψ denotes as yaw of the vehicle, $\dot{x}$ denotes as the speed of longitudinal motion in the x-direction and $\omega_{L/R}$ are the angular speed of the left and right tracks of the vehicle.

$$F_{L/R} = F_{max}\left[1 - \frac{\left(\frac{k}{l}\right)}{|i|}\left(-e^{-|i|}\right)\right]\text{sign}(i) \quad (4)$$

$$F_{max} = A\tau_{max} = A[C + P\tan(\psi)] \quad (5)$$

$$i = \frac{V_j}{r\omega} \quad (6)$$

$$V_{jL} = [\dot{x} - b\dot{\psi}] - r\omega_L \quad (7)$$

$$V_{jR} = [\dot{x} + b\dot{\psi}] - r\omega_R \quad (8)$$

Moreover, Equation (9) shows the longitudinal resistive forces occurred by the interaction between the soil and tracks of the vehicle where μ_x is the longitudinal coefficient of friction and g is the gravitational acceleration. Meanwhile, the lateral friction force per unit length that is occurred by the lateral soil shear distribution force acting on the tracked vehicle is determined by (10) where μ_y represents the lateral friction coefficient and l is the half length of the tracked vehicle.

$$R = \frac{\mu_x mg}{2} \quad (9)$$

$$f_y = \frac{\mu_y mg}{2l} \quad (10)$$

The lateral friction force components, F_y occurred in two direction which are forces following and opposite the lateral direction, F_{y1}, F_{y2} that enclosed in (11) and (12). The tracked vehicle's movement is obtained by using right-hand rules which specify that the positive lateral force is applied in the left direction. Therefore, the lateral friction force of the tracked vehicle obtained in (13) is derived by adding all the lateral forces involved and substituting (11) and (12).

$$F_{y1} = f_y(l - d_s) \quad (11)$$

$$F_{y2} = f_y(l + d_s) \quad (12)$$

$$F_y = 4f_y d_s \quad (13)$$

Furthermore, the local coordinates of tracked vehicle's movement should be transform to global coordinates for observing the translational mobility on a real system. The conversion equations for the longitudinal direction and lateral direction are enclosed in (14) and (15) where $\dot{x}$ is the velocity acting at x-axis, $\dot{y}$ is the velocity acting at y-axis, and ψ denotes the yaw.

$$\dot{X} = \dot{x}\cos\psi - \dot{y}\sin\psi \quad (14)$$

$$\dot{Y} = \dot{x}\sin\psi + \dot{y}\cos\psi \quad (15)$$

On top of that, since friction models were developed only for a certain direction of motion, a more comprehensive model is required when the velocities are varying. Therefore, Equation (16) is included to the vehicle model which the vector G denotes the resultant of the friction and the input force acting on the vehicle. This Equation explained that when the friction force is larger than the tractive force, the vehicle remains stationary. The parameters of the real tracked vehicle used in this study are shown in Table 1

$$G(F, f, \dot{x}) = \begin{cases} F - f\text{sign}(\dot{x}) & \dot{x} \neq 0 \\ 0 & \dot{x} = 0, |F| \leq f \\ F - f\text{sign}(F) & \dot{x} = 0, |F| \geq f \end{cases} \quad (16)$$

TABLE 1. Parameters of the tracked vehicle

Vehicle Parameter	Value
Initial velocity, $V_0\ (m/s)$	0.79
Left sprocket speed, $\omega_L\ (rad/s)$	7.65, 3.07
Right sprocket speed, $\omega_R\ (rad/s)$	2.83, 7.47
Gravitational acceleration, $g\ (m/s^2)$	9.81
Radius of sprocket, $r\ (m)$	0.15
Contact area between soil and tracked vehicle, $A\ (m^2)$	0.129

continue ...

... cont.

Apparent cohesion of the soil, $c(Pa)$	$68.95e^{-2}$
Modulus of soil deformation, $k\ (m)$	0.006
Longitudinal friction coefficient, μ_x	0.2
Lateral friction coefficient, μ_y	0.55
Half-width of the tracked vehicle, $b\ (m)$	0.369
Mass moment inertia, $I\ (kgm^2)$	54.55
Mass of the tracked vehicle, $m\ (kg)$	150
Half-length of the tracked vehicle, $l\ (m)$	0.58
Angle of internal friction, Ø (rad)	0.5934

DEVELOPMENT AND VALIDATION OF DC MOTOR MODEL AND CONTROLLER

This section describes the methodology for developing the independent speed controller using a linear interpolation method by obtaining and validating in-track DC motors characteristics. The DC motor model and its inverse database model was developed in MATLAB 2021. The modelling and validations of the in-track DC motor is further discussed.

MODELLING AND VALIDATION OF AN IN-TRACK DC MOTOR

This study employs DC motors to control the vehicle's movement, which is set on the left and right tracks of the tracked vehicle. . This study has been covered in detail in previous work by authors (Ruslan et al. 2023). Modelling and identification of the DC motor system on individual tracks is developed by establishing the correlation between the input byte, which ranges from 0 to 255, supplied to the DC motor, and the resulting vehicle speed (V), as well as the turning radius (ρ) produced by the tracked vehicle. In this system, the input byte is obtained from the pulse width modulation (PWM) value supplied to regulate the DC motor speed. The motor is controlled by inputting voltage to two different channels, namely Channel 2 and Channel 4, which control the vehicle speed and turning radius of the vehicle, respectively. However, this voltage will differ depending on the total capacity of the battery used on-board. Therefore, a more general approach using input byte for an 8-bit system is used. To achieve this relationship, variations in vehicle speed and turning radius of the varying input bytes are recorded. The vehicle speed data is acquired through the rotational movement of its tracks as shown in (17) while the turning radius is obtained from centre point to the path travelled by the vehicle. Figure 2 shows the complete experimental setup while Figure 3 shows an overview of the methods required to model the DC motor.

$$V = \omega_{track} \times r_{sprocket} \tag{17}$$

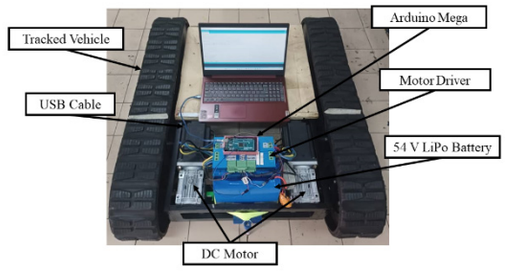

FIGURE 2. Experimental setup of the tracked vehicle

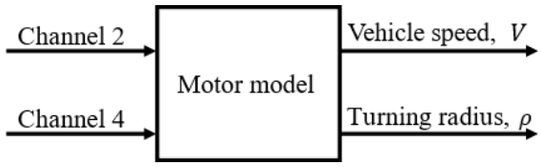

FIGURE 3. Estimation of vehicle speed and turning radius based on byte characteristics

The relationship of the vehicle speed and turning radius are determined based on the characteristics of the DC motor as shown in Figure 4 (a), (b) and (c). These graphs are observed in three different path which is forward, cornering left and right by manipulating the speeds of both tracks of the vehicle. On top of that, through these graphs, it is observed that all the path involved produced linear relationship of the vehicle speed, turning radius and byte for DC motor. Based on Figure 4 (a) the vehicle speed is increased with the increased of the input byte of the DC motor. Next, for turning manoeuvring, increasing Channel 2 value has similar effect observed during forward manoeuvring: i.e.; increase in vehicle travelling speed. Main characteristic can be observed in varying Channel 4 values. The sign in Channel 4 dictates the turning direction, where positive is for right turning and negative is for left turning. While the sign dictates its turning direction, the magnitude of Channel 4 dictates its turning radius.

Increasing Channel 4 byte magnitude will decrease the turning radius. Therefore, larger Channel 4 will cause the vehicle to have smaller turning radius, resulting in

sharper cornering. This relationship can be illustrated in Figure 4 (b) and (c) for right and left cornering, respectively. In summary, it can be observed from the graphs that the speed of the vehicle is directly proportional to Channel 2 and the radius of turn is inversely proportional to Channel 4.

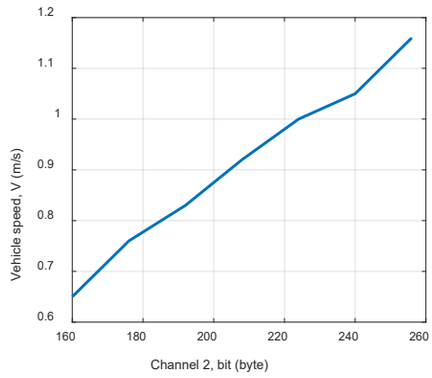

(a) Vehicle speed against byte relationship for straight path

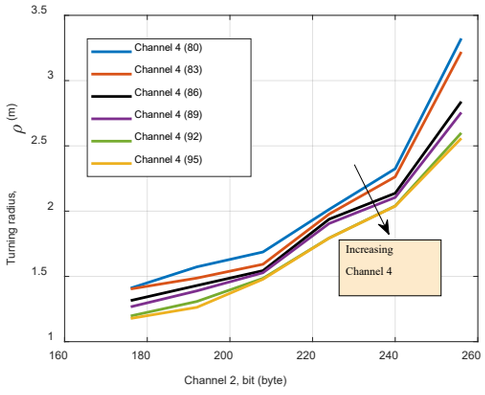

(b) Turning radius against byte relationship for right cornering

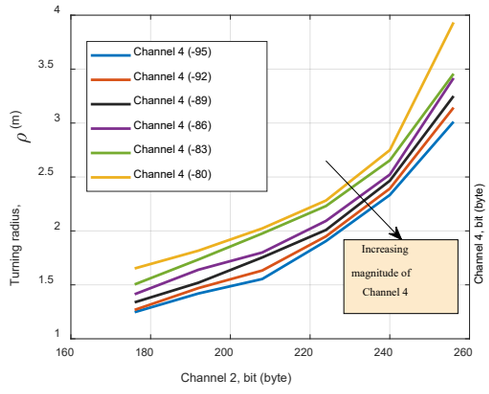

(c) Turning radius against byte relationship for left cornering

FIGURE 4. Characteristic of DC motor

In addition, the characteristics of the DC motor model is validated by comparing the actual turning radius against the predicted turning radius and the vehicle's speed. The comparison on the vehicle speed is measured when the vehicle travelled in the straight path while the turning radius is measured when the vehicle manoeuvres in right and left direction. The validated results on DC motor characteristics are shown in the Figure 5 (a), (b) and (c) for every type of path the vehicle travelled. The characteristics of the DC motor is validated when the actual response on vehicle speed and turning radius behaves likely to the predicted response of the vehicle. Figure 5 (a) shows the graph validation of vehicle speed against byte (channel 2) for straight path. Based on this graph, it shows that the relationship of the vehicle speed and byte is linearly increased and for this straight path, it is only affected in the setting of the channel 2 and the setting of channel 4 remains zero. The root mean square (RMS) of the percentage error between the predicted and actual vehicle speed is then determined which obtained 1.8%.

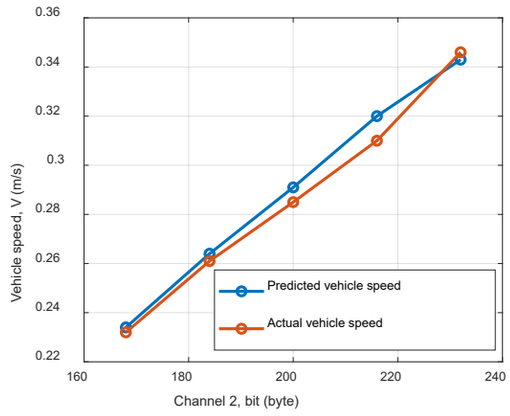

(a) Vehicle speed against byte relationship for straight path

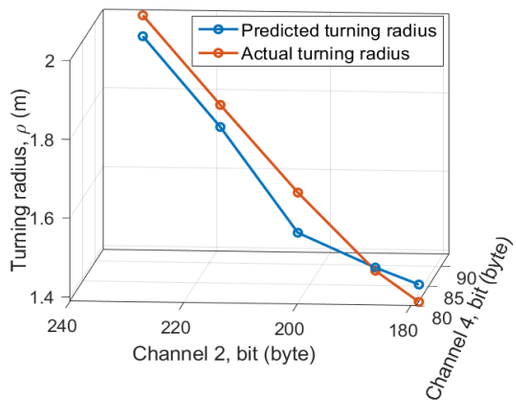

(b) Turning radius against byte relationship for right cornering

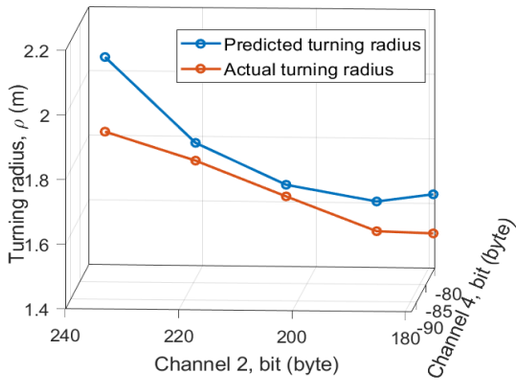

(c) Turning radius against byte relationship for left cornering

FIGURE 5. Validation of DC motor characteristics

Next, Figure 5 (b) shows the graph on the turning radius against channel 2 and 4 for right cornering. Upon setting the value of byte (channel 2 and 4), the turning radius of the vehicle is observed to decrease as the value of input byte on channel 2 and 4 increased. Based on this graph, the RMS of the percentage error between the predicted and actual turning radius during right turns is 3.7%.

Furthermore, during the left turn of the vehicle, a noticeable trend is observed: when the magnitude of input byte for Channel 2 and Channel 4 increases, the turning radius of the vehicle decreases as depicted in Figure 5 (c). As indicated by the graph, the RMS of the percentage error calculated for the left turn of the vehicle is 7.1%.

DEVELOPMENT AND VALIDATION OF DC MOTOR CONTROLLER

According to the previously obtained correlation between vehicle speed, turning radius, and the byte value for DC motors, a speed controller for both DC motors is developed. An inverse database was developed from the motor characteristics in Figure 4 (a), (b), (c) to predict the required byte (Channel 2 and Channel 4) for any predicted motor speed, ($\omega_{desired}$) as shown in Figure 6 (a), (b), (c) for the forward, left and right manoeuvrings of the vehicle.

With this approach, the byte for channel 2 and 4 required to get any predicted track speed may be properly predicted using a linear interpolation method. The data points from the motor characteristics in Figure 6 (a), (b) and (c) will be used with the linear interpolation approach. Each segment between the data points will be regarded as a linear region. At any given arbitrary point (x_a), the corresponding arbitrary value (y_a) will be determined by interpolating between the pair of data points, namely $((x_i, y_i)$ and $(x_f, y_f))$, that lie in between them as stated in (18).

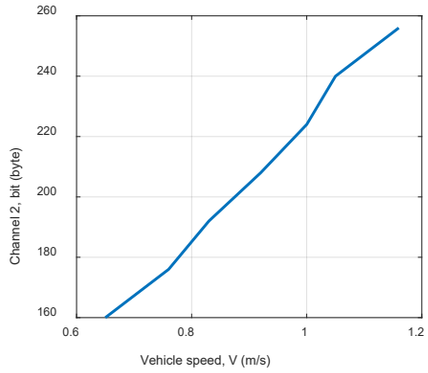

(a) Straight path

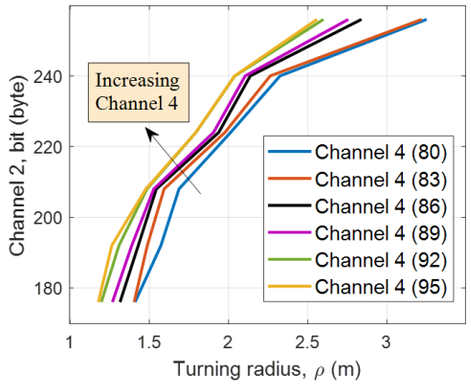

(b) Right cornering

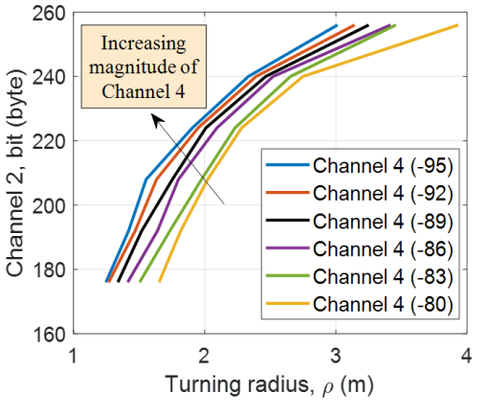

(c) Left cornering

FIGURE 6. Inverse model database developed from speed-byte characteristics

$$y_a = y_i + (x_a - x_i)\frac{(y_f - y_i)}{(x_f - x_i)} \tag{18}$$

This approach will be employed to create a precise model of the DC motor. In addition, the resulting structure of DC motor controller is shown in Figure 7 for those three types tracked vehicle manoeuvrings. Meanwhile, Equations (19) and (20) derived the relationship between the vehicle's turning radius and its speed in the context of the inverse kinematic model when the predicted angular speed is applied.

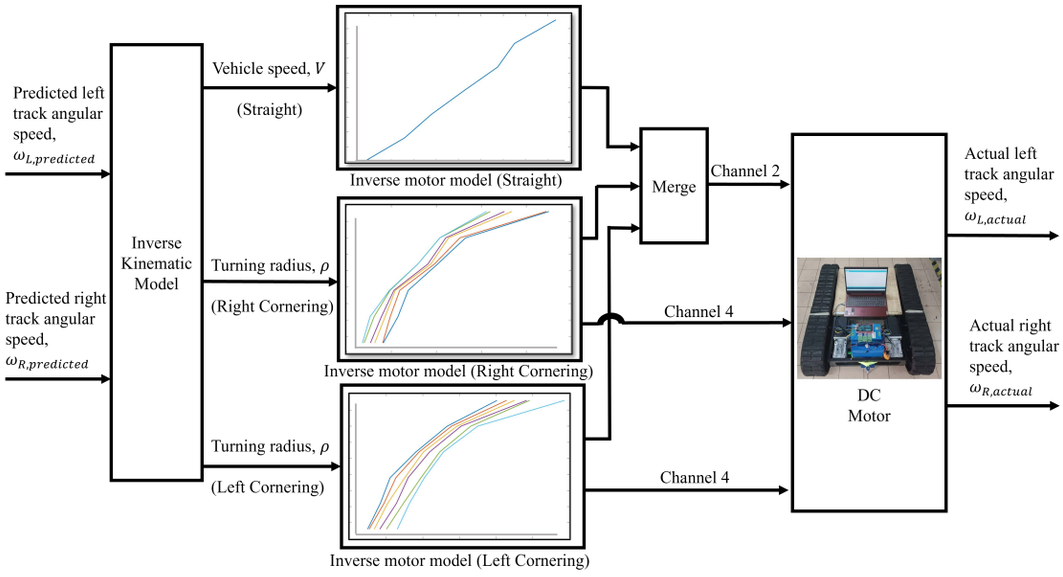

FIGURE 7. Control structure for in-track-DC motor of the tracked vehicle

$$V = \frac{\omega_L + \omega_R}{2} \tag{19}$$

$$\rho = \frac{B}{2}\left(\frac{r\omega_L + r\omega_R}{r\omega_L - r\omega_R}\right) \tag{20}$$

Additionally, the generated motor model with open-loop control as depicted in Figure 7, is validated by comparing the actual and predicted speeds of both left and right tracks while varying the input byte of the DC motor. The actual speed is determined by gathering the tracked vehicle's angular speed data throughout the experiment, whereas the predicted speed is the total speed that should be achieved by adjusting the input byte that obtained from the vehicle speed and turning radius of the vehicle. Based on Figure 8 (a) and (b), the proposed independent DC motor controller is validated by calculating its RMS of the percentage error for both right and left cornering. The RMS of the percentage error for right cornering on the angular speed of left and right tracks are 8.14% and 5.46% respectively. Meanwhile, for the left cornering, the recorded RMS of the percentage error for angular speed of left and right tracks are 3.11% and 7.72% respectively. This shows that the proposed independent DC motor controller have a good agreement between the predicted and actual angular speed of tracks produced.

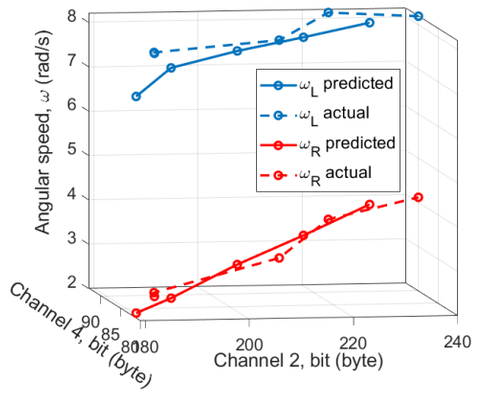

(a) Right cornering

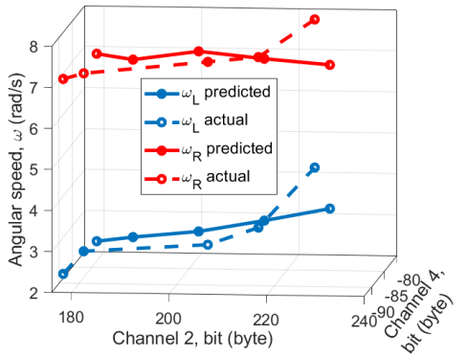

(b) Left cornering

FIGURE 8. Validation of angular speed against bytes (Channel 2 and 4)

VALIDATION OF DEVELOPED VEHICLE MODEL FOR TRACKED VEHICLE

Based on the developed vehicle model as discussed in Section3, the model is then validated by comparing it to the experimental response on the tracked vehicle's trajectory as illustrated in Figure 9. In the validation process, both the simulation and experimental vehicle are supplied with input to have two manoeuvrings, namely left and right cornering. For the left manoeuvring, the predicted angular speed of both left and right tracks are set for $\omega_L = 7.65$ rad/s, $\omega_R = 2.83$ rad/s, and $\omega_L = 3.07$ rad/s, $\omega_R = 7.47$ rad/s for the right manoeuvring. In the experimental vehicle, the implemented DC motor speed controller will be employed, and the vehicle's response in X-Y global coordinates will be obtained using the MPU 6050 accelerometer. Meanwhile, for the simulation, the developed tracked vehicle model in Simulink will have its predicted angular speed of both tracks to generate the vehicle response in X-Y global coordinates. Figure 10 (a) and (b) show the comparison between the X-Y global coordinates for tracked vehicle simulation and the actual vehicle response measured experimentally. Based on Figure 10 (a) and (b), the RMS of the percentage error for the trajectories X-Y global coordinates for right and left cornering are 10.60% and 12.66% respectively. These errors are contributed by various factors. Since the characteristics of DC motor estimation was used, associated error from this model was carried forward within the motor controller, power powertrain, combined with internal friction within the vehicle setup, and lastly to the actual trajectory realized on the vehicle. From the response for both manoeuvrings, responses from the developed vehicle model simulation agrees with the actual vehicle response. This validates the vehicle model as well as the independent motor control being used on the tracked vehicle.

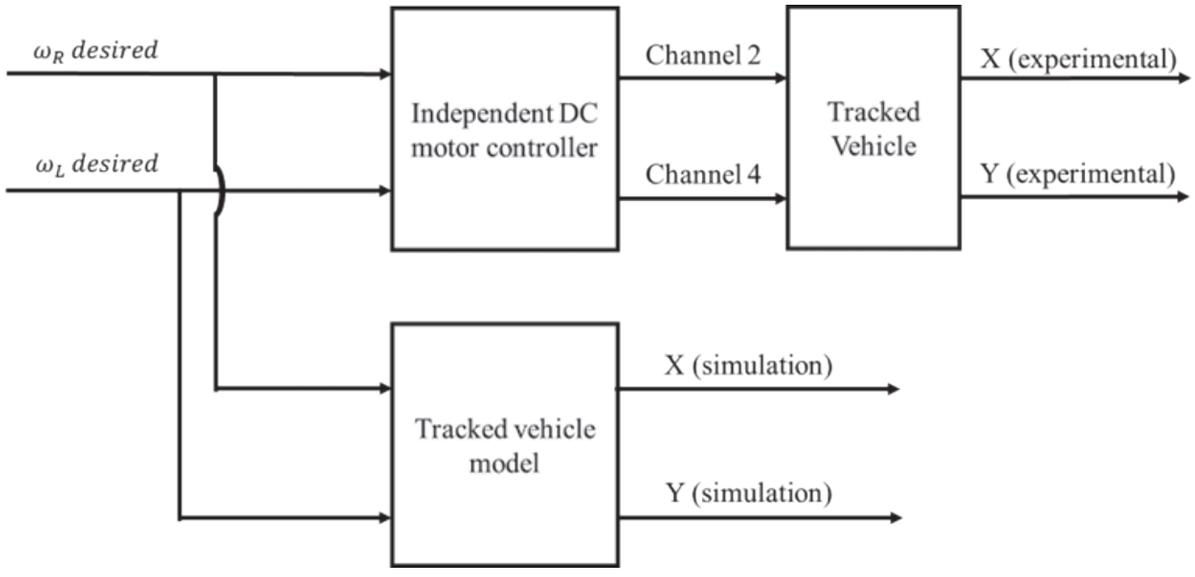

FIGURE 9. Validation diagram for tracked vehicle

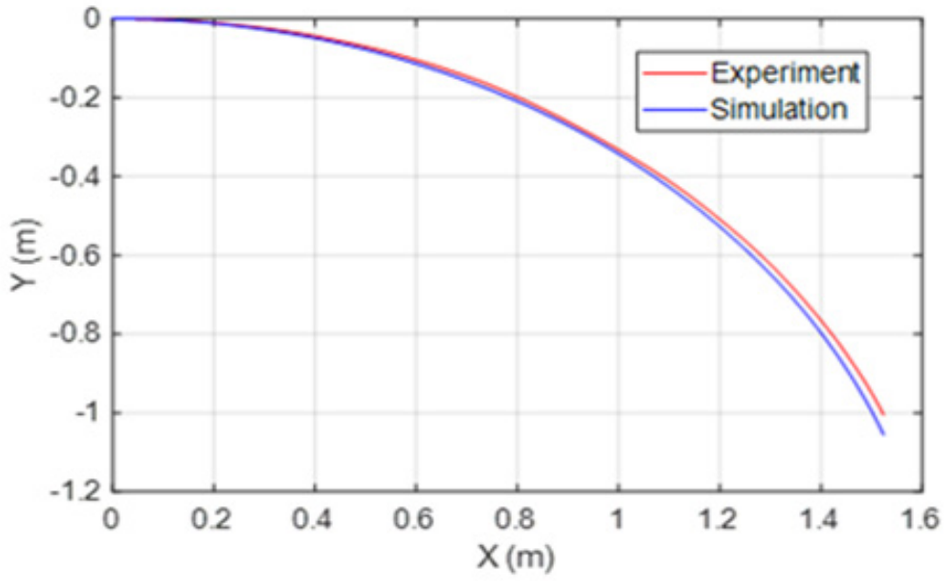

(a) Right cornering

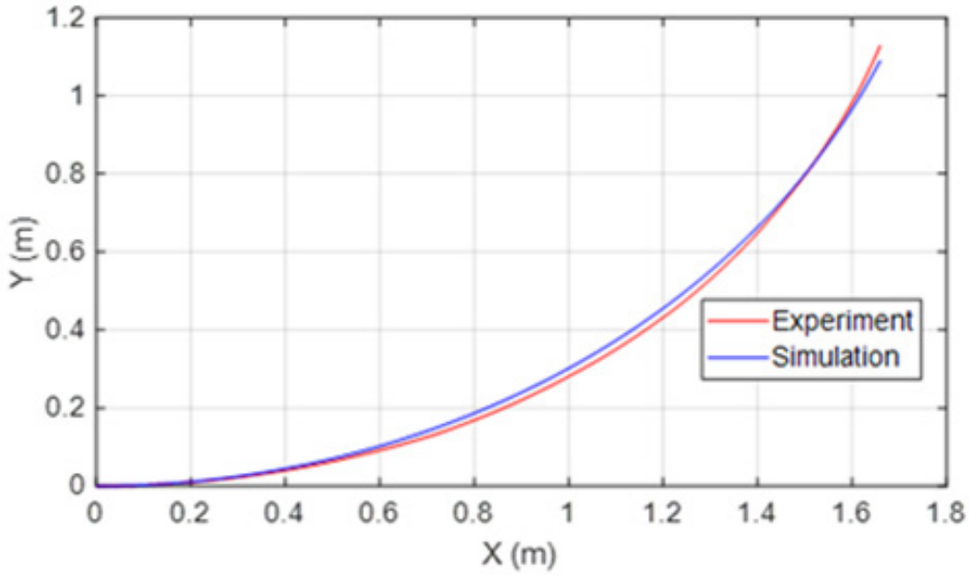

(b) Left cornering

FIGURE 10. Trajectory of the tracked vehicle

CONCLUSION

A dynamic vehicle model of tracked vehicle was developed in Simulink based on the equations of forces involved. A speed controller of the DC motor for both left and right tracks was developed based on the obtained characteristics. Next, the validation on DC motor controller was done by comparing the predicted and actual value of turning radius and tracked vehicle's speed. The validation process of the dynamic tracked vehicle model was obtained experimentally and by simulations for its trajectories. The percentage error produced for the right and left turns of the vehicle are

10.90% and 12.66% respectively which shows the model is able to follow the path in real conditions. The improvement can be done to get the least lateral errors by applying various of filters in order to remove unnecessary noise that occurs during the experiment.

ACKNOWLEDGEMENT

A high appreciation dedicated to Ministry of Higher Education, Malaysia for their financial support, technical advices and the use of their research facility for this research through Fundamental Research Grant Scheme: FRGS/1/2021/TK02/UPNM/02/2 and Universiti Pertahanan Nasional Malaysia for support in facilities.

DECLARATION OF COMPETING INTEREST

None.

REFERENCES

Adli, M. S., Mohamad Hanif, N. H. H., & Tohara, S. F. T. 2018. Brushless DC motor speed controller for electric motorbike. *International Journal of Power Electronics and Drive Systems 9*(2): 859–864.

Ahmadi, M., Polotski, V., & Hurteau, R. 2000. Path tracking control of tracked vehicles. *Proceedings-IEEE International Conference on Robotics and Automation*, 3(April): 2938–2943.

Al-Jarrah, A. 2019. Controlling a skid-steered tracked mobile robot with slippage using various control schemes. *2019 20th International Conference on Research and Education in Mechatronics (REM)* 5: 1–7.

Auliansyah, F., Sutedjo, Asrarul Qudsi, O., & Ferdiansyah, I. 2020. Controlling speed of brushless dc motor by using fuzzy logic controller. *Proceedings - 2020 International Seminar on Application for Technology of Information and Communication: IT Challenges for Sustainability, Scalability, and Security in the Age of Digital Disruption, ISemantic 2020*, 298–304.

Hu, K., & Cheng, K. 2023. Trajectory planning for an articulated tracked vehicle and tracking the trajectory via an adaptive model predictive control. *Electronics (Switzerland):* 12(9).

Jiao, J., Chen, J., Qiao, Y., Wang, W., Wang, M., Gu, L., & Li, Z. 2018. Adaptive sliding mode control of trajectory tracking based on DC motor drive for agricultural tracked robot. *Nongye Gongcheng Xuebao/Transactions of the Chinese Society of Agricultural Engineering* 34(4): 64–70.

Le, A. T., Rye, D. C., & Durrant-whyte, H. F. 2006. Estimation of back-soil interactions for autonomous tracked vehicles. *April 1997*, 1388–1393.

Ma'Arif, A., Iswanto, Raharja, N. M., Rosyady, P. A., Baswara, A. R. C., & Nuryono, A. A. 2020. Control of DC motor using Proportional Integral Derivative (PID): Arduino hardware implementation. *Proceeding - 2020 2nd International Conference on Industrial Electrical and Electronics, ICIEE 2020*, 74–78.

Naik, A. K., Kar, S. K., & Sahu, B. K. 2021, January 8. Speed control of DC motor using linear and non-linear controllers. *1st Odisha International Conference on Electrical Power Engineering, Communication and Computing Technology, ODICON 2021*.

Ruslan, N. A. I., Amer, N. H., Hudha, K., Kadir, Z. A., Ishak, S. A. F. M., & Dardin, S. M. F. S. M. 2023b, October. Independent Speed Controller for Integrated Motion Control of Tracked Vehicle with In-Track Motors. In *23rd International Conference on Control, Automation and Systems (ICCAS):* 478-482. IEEE.

Sabiha, A. D., Kamel, M. A., Said, E., & Hussein, W. M. 2022. ROS-based trajectory tracking control for autonomous tracked vehicle using optimized backstepping and sliding mode control. *Robotics and Autonomous Systems* 152.

Saito, M., Tamaki, K., Nishiwaki, K., Nagasaka, Y., & Motobayashi, K. 2013. Development of robot combine harvester for beans using CAN bus network. *IFAC Proceedings Volumes (IFAC-PapersOnline):* 4(PART 1): 148–153.

Salah, M., & Al-Jarrah, A. 2019. Robust backstepping control for tracked vehicles under the influence of slipping and skidding. *Proceedings of the 2019 20th International Conference on Research and Education in Mechatronics, REM 2019*, *5*, 1–6.

Sebastian, B., & Ben-Tzvi, P. 2019. Physics Based path planning for autonomous tracked vehicle in challenging terrain. *Journal of Intelligent and Robotic Systems: Theory and Applications* 95(2): 511–526.

Sivakumar, P., Reginald, R., Venkatesan, G., Viswanath, H., & Selvathai, T. 2017. Configuration study of hybrid electric power pack for tracked combat vehicles. *Defence Science Journal* 67(4): 354–359.

Sultan, N. M., Md Zain, B. A., Anuar, F. F., Yahya, M. S., Latif, I. A., Hat, M. K., & Al-alimi, S. 2019. Modeling and speed control for sensorless DC motor BLDC based on real time experiment. *International Journal of Integrated Engineering* 11(8): 55–64.

Ugenti, A., Galati, R., Mantriota, G., & Reina, G. 2023. Analysis of an all-terrain tracked robot with innovative suspension system. *Mechanism and Machine Theory* 182.

Vikhe, P. S., Shukla, B. S., Kadu, C. B., & Mandhare, V. V. 2019. Speed control of BLDC motor using open loop, PID controller and neural network. *International Journal of Engineering and Advanced Technology* 9(1): 2210–2213.

Wang, H., Zhang, Y., Wang, X., & Feng, Y. 2022. Cascaded continuous sliding mode control for tracked mobile robot via nonlinear disturbance observer. *Computers and Electrical Engineering* 97.

Wenju, M., Heng, L., Wei, H., Fuzeng, Y., & Zhijie, L. 2022. Development of a combined orchard harvesting robot navigation system. *Remote Sensing* 14(3).

Yang, H., Xu, X., & Hong, J. 2023. Automatic parking path planning of tracked vehicle based on improved A□ and DWA algorithms. *IEEE Transactions on Transportation Electrification* 9(1): 283–292.

Yang, Y., Han, Y., Li, S., Yang, Y., Zhang, M., & Li, H. 2023. Vision based fruit recognition and positioning technology for harvesting robots. *Computers and Electronics in Agriculture* 213.

Zou, T., Angeles, J., & Hassani, F. 2018. Dynamic modeling and trajectory tracking control of unmanned tracked vehicles. *Robotics and Autonomous Systems* 110: 102–111.